# Transmission Electron Microscopic Studies of $LiNb_{0.5}Ta_{0.5}O_3$ Films Deposited on Sapphire Substrates by Thermal Plasma Spray CVD (Microstructure of $LiNb_{0.5}Ta_{0.5}O_3$ Films Deposited by Thermal Plasma Spray CVD)

Junko Shibata[1, *], Hironori Yamamoto[2], Sergei A. Kulinich[2], Takahisa Yamamoto[2],
Kazuo Terashima[2], Toyonobu Yoshida[3] and Yuichi Ikuhara[1]

[1]*Engineering Research Institute, School of Engineering, The University of Tokyo, Tokyo 113-8656, Japan*
[2]*Department of Advanced Materials Science, Graduate School of Frontier Sciences, The University of Tokyo, Tokyo 113-8656, Japan*
[3]*Department of Materials Engineering, School of Engineering, The University of Tokyo, Tokyo 113-8656, Japan*

Cross sections and plan views of $LiNb_{0.5}Ta_{0.5}O_3$ films were investigated mainly by high-resolution transmission electron microscopy. These films were deposited on (0001) sapphire substrates by thermal plasma spray chemical vapor deposition method at various feeding rates of liquid raw materials. It was found that the crystallinity and the preferential orientation of the LNT films depend on the feeding rate. The LNT film formed at the feeding rate of 7 mL/min was epitaxially grown on the substrate, and the orientation relationship between the film and the substrate was $(0001)_{LNT}//(0001)_{sapphire}$, $[11\bar{2}0]_{LNT}//[11\bar{2}0]_{sapphire}$. The LNT films fabricated at the higher and the lower feeding rate were polycrystalline. These films included twin crystals and other phases such as $Li(Nb, Ta)_3O_8$. The calculations based on the coincidence of reciprocal lattice points revealed that the epitaxial orientation relationships observed by transmission electron microscopy satisfied the geometrically optimal coherency across the interface.

## 1. Introduction

LiNbO₃ (LN) and LiTaO₃ (LT) have been applied for electrical and optical devices, since they exhibit ferroelectricity, piezoelectricity and pyroelectricity. These LN and LT have been synthesized in the single crystal form by such a Czochralski method, and have been actually used for surface acoustic wave (SAW) devices or guided-wave optics. $LiNb_xTa_{1-x}O_3$(LNT), which is a solid solution of LN and LT, is also promising materials for further applications. There is a possibility that the LNT shows superior properties to LN and LT, although the physical properties of the LNT material have not been clarified.

Single crystal films of LN and LT are deposited by various methods such as liquid phase epitaxy (LPE),[1] metal organic chemical vapor deposition (MOCVD),[2, 3] pulsed laser deposition (PLD),[4–8] sol–gel method[9–11] and sputtering technique.[12] However, only a few papers have been reported for processing of LNT. In particular, in the case of many composition of Ta ($x > 0.4$), high quality film has not been successfully fabricated. This is because the melting point of the LNT is higher as the amount of Ta is larger. T. Kawaguchi *et al*. reported that LNT films were grown on LN substrates by LPE, but the crystallinity of the films degraded at $x > 0.3$.[13] S. D. Cheng *et al*. formed LNT films ($0 < x < 1$) on Si(111) substrates by sol–gel method.[14] In this research, highly *c*-axis oriented films were obtained in the composition range of $0 < x < 0.33$ and the degree of the orientation was found to be relatively low when $0.5 < x < 1$.

On the other hand, thermal plasma spray chemical vapor deposition (CVD) method has advantages of producing the films at high speed ($\sim$ 1 μm/min) in a large area, and controlling the chemical composition of multi-component materials. We have previously applied the thermal plasma flash evaporation method to grow the superconducting oxide $YBa_2Cu_3O_{7-y}$ films with high critical temperature ($T_C$).[15–17] Later, it was also reported that LN films were successfully fabricated by the thermal plasma spray CVD.[18]

In the present work, LNT films were deposited by the thermal plasma spray CVD with changing a feeding rate of liquid raw solution, and their microstructures were investigated to clarify the effect of the feeding rate on the film quality.

## 2. Experimental

The LNT films were deposited by thermal plasma spray CVD method at the various feeding rates. The details of the process were described in the previous papers.[19,20] Lithium-niobium and lithium-tantalum alkoxide metalorganic solutions [$LiNb(OR)_6$ and $LiTa(OR)_6$ in 3-methylbutyl acetate as a solvent, which were commercially available for dip coatings at Kojundo Chemical Laboratory Co., Japan] were used for liquid precursors. The concentration of metals in each individual precursor solution corresponded to 3mass% LiNbO₃ and LiTaO₃ respectively. These solutions were then mixed in molar Nb:Ta ratio of 1:1. As-received optically polished sapphire(0001) substrates (Earth Chemicals Ltd., Japan) were ultrasonically cleaned and rinsed with aceton and ethanol. The

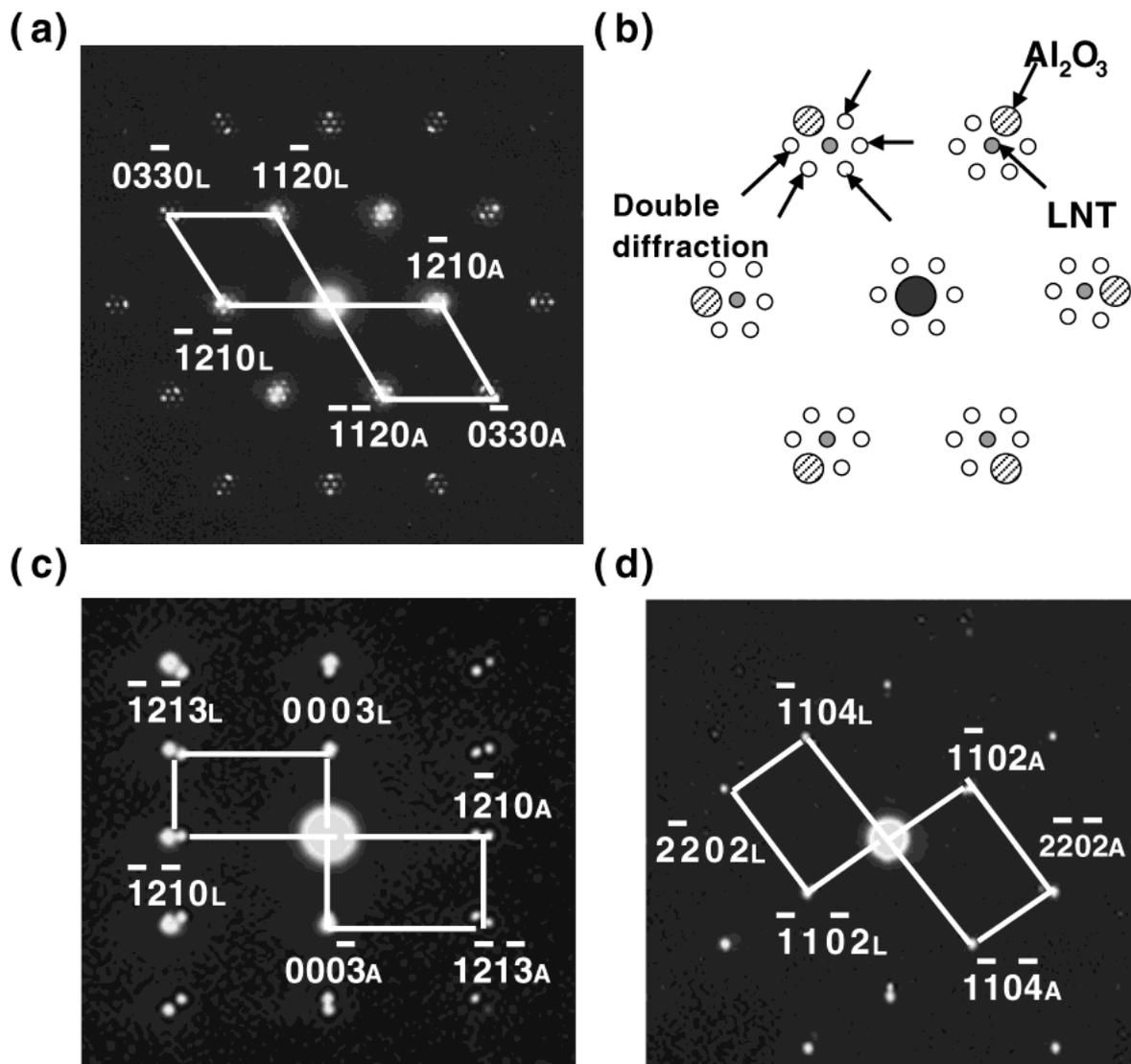*Current address: Superconductivity Research Laboratory, ISTEC, Tokyo 135-0062, Japan. E-mail: jshibata@istec.or.jp

Fig. 1    Selected-area electron diffraction patterns (SAEDPs) of sample C taken along three directions of (a) $[0001]_{Al_2O_3}$; (b) $[10\bar{1}0]_{Al_2O_3}$; (c) $[11\bar{2}0]_{Al_2O_3}$. The orientation relationship between the LNT film and the sapphire substrate is as follows: $[11\bar{2}0]_{LNT}//[11\bar{2}0]_{Al_2O_3}$; $(0001)_{LNT}//(0001)_{Al_2O_3}$.

substrate temperature (933 K) was controlled within the accuracy $\pm 15$ K and was measured by detecting infrared radiation from the reverse side of the substrate through an optical fiber, which made it possible to monitor the substrate temperature directly in real time.

The liquid precursors containing metalorganic compounds were introduced as a mist into the oxygen-argon plasma through the stainless-steel probe tube. Carrier argon gas (3 L/min), inner argon gas (5 L/min) and spray argon gas (3.6 L/min), along with tangential oxygen gas (45 L/min), were introduced into the chamber through and around the injection probe. The total pressure in the chamber was maintained at $2.00 \times 10^4$ Pa. Once in the plasma, the liquid precursors were evaporated, decomposed, and reacted in the boundary layer over the substrate to form LNT deposit. The feeding rate of the liquid raw materials was controlled in the range from 0.5 to 10 mL/min. We name the films formed at the feeding rate of 0.5, 1, 7 and 10 mL/min as 'sample A', 'sample B', 'sample C' and 'sample D', respectively.

Crystallinity and orientation of the LNT films depend on the other conditions than the feeding rate, such as the substrate temperature and the pressure in the chamber. In the present work, these other conditions were controlled within the range in which the epitaxial growth of the film occurred.

The phase composition and the preferential orientation of the films were investigated using conventional $\theta$–$2\theta$ scan X-ray diffraction method. The $c$-axis planar alignment of the films was determined by rocking curve analysis. The rocking curve full width at half maximum (FWHM) value obtained from sapphire substrate was of $0.04°$. The chemical composition of the films was analyzed by inductively coupled plasma atomic emission spectroscopy (ICP-AES) after the samples had been completely dissolved in HF and $H_2SO_4$.

Transmission electron microscopy (TEM) specimens for individual films were prepared using standard techniques including mechanical grinding to a thickness of 60–80 μm, dimpling to 15–20 μm and ion beam milling to electron transparency at 4–5 kV. During the ion milling, when the incident ion beam was parallel to the interface between the film and the substrate, the specimen was rotated quickly to protect
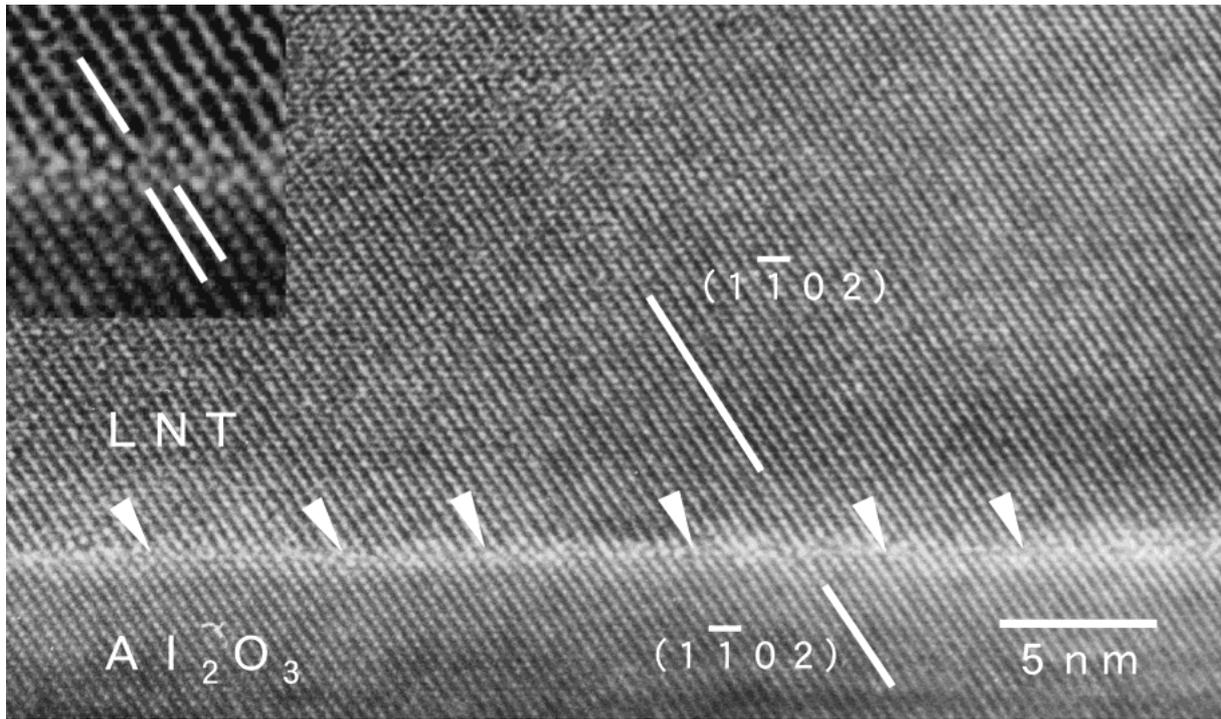
Fig. 2 High-resolution transmission electron microscopic(HRTEM) image of sample C, observed from the direction of [11$\bar{2}$0]$_{\text{LNT}}$//[11$\bar{2}$0]$_{\text{Al}_2\text{O}_3}$. Geometrical misfit dislocations are indicated by arrows.

Table 1 Rocking curve FWHM values for (0006)LNT peak.

| Sample | Feeding rate, mL/min | FWHM, degree |
|---|---|---|
| Sample A | 0.5 | 0.57 |
| Sample B | 1 | 0.41 |
| Sample C | 7 | 0.17 |
| Sample D | 10 | 0.23 |

the selective thinning along the LNT film/sapphire interface. TEM used in this work was Hitachi-9000NAR with the point-to-point resolution of 0.19 nm operating at 300 kV. High-resolution transmission electron microscopy (HRTEM) images were obtained from three directions: two cross-sectional views (parallel to [11$\bar{2}$0]$_{\text{Al}_2\text{O}_3}$ and [10$\bar{1}$0]$_{\text{Al}_2\text{O}_3}$) and plan view (parallel to [0001]$_{\text{Al}_2\text{O}_3}$).

## 3. Results and Discussion

### 3.1 Effect of feeding rate on microstructures

Rocking curve analysis revealed the crystallinity of the LNT films was influenced by the feeding rate of liquid raw solution. FWHMs of (0006)$_{\text{LNT}}$ peak are listed in Table 1. It is noted that FWHM for sample C deposited at the feeding rate of 7 mL/min, which is in the middle range from 0.5 mL/min to 10 mL/min, is the smallest among them. This implies that the sample C has the best crystallinity. We observed these samples by using TEM in order to clarify the phase compositions and the orientation relationships of the films especially at the LNT/Al$_2$O$_3$ interfaces in detail.

Figures 1(a), (c) and (d) show selected-area electron diffraction patterns (SAEDPs) of sample C obtained from three directions of: (a) [0001]$_{\text{Al}_2\text{O}_3}$; (c) [10$\bar{1}$0]$_{\text{Al}_2\text{O}_3}$; (d)

[11$\bar{2}$0]$_{\text{Al}_2\text{O}_3}$, respectively. According to these diffraction patterns, the orientation relationship (OR) between LNT film and the (0001) basal plane of the sapphire is the following:

$$(0001)_{\text{LNT}}//(0001)_{\text{Al}_2\text{O}_3}, \quad [11\bar{2}0]_{\text{LNT}}//[11\bar{2}0]_{\text{Al}_2\text{O}_3} \quad (I)$$

In Fig. 1(a), double diffraction spots are visible around fundamental spots by reflections of the sapphire planes. Figure 1(b) shows an interpretation on the double diffraction spots in Fig. 1(a).

Figure 2 shows a HRTEM micrograph of sample C, observed from the direction of [11$\bar{2}$0]$_{\text{LNT}}$//[11$\bar{2}$0]$_{\text{Al}_2\text{O}_3}$. This figure shows that (0001)$_{\text{LNT}}$ planes are parallel to the (0001)$_{\text{Al}_2\text{O}_3}$ planes of sapphire, and [0001]$_{\text{LNT}}$ normal to the interface. This film is epitaxially grown and there is neither amorphous layer nor other phase with different chemical composition at the interface between the film and the substrate. The misfit parameter between (1$\bar{1}$02)$_{\text{LNT}}$ and (1$\bar{1}$02)$_{\text{Al}_2\text{O}_3}$ along the [10$\bar{1}$0]$_{\text{Al}_2\text{O}_3}$ direction is estimated to be 8.4%. In such a system with large lattice mismatch (a misfit parameter larger than 5%) but with weak interfacial bondings, a set of geometrical misfit dislocations are present which are obtained from overlap of two dissimilar lattice spacings.[21] These geometrical misfit dislocations accommodate the mismatch between the two components from the very initial stages. Geometrical misfit dislocations are thus seen, which occur periodically at every eleven (1$\bar{1}$02)$_{\text{LNT}}$ planes, corresponding to about twelve (1$\bar{1}$02)$_{\text{Al}_2\text{O}_3}$ planes, as shown in the inset.

Figure 3 shows the HRTEM micrograph of sample C, taken along the direction of [10$\bar{1}$0]$_{\text{LNT}}$//[10$\bar{1}$0]$_{\text{Al}_2\text{O}_3}$. The misfit parameter between (1$\bar{2}$10)$_{\text{LNT}}$ and (1$\bar{2}$10)$_{\text{Al}_2\text{O}_3}$ is 7.6%. Although the interface looks like incoherent interface, there must be geometrical misfit dislocations along the interface.

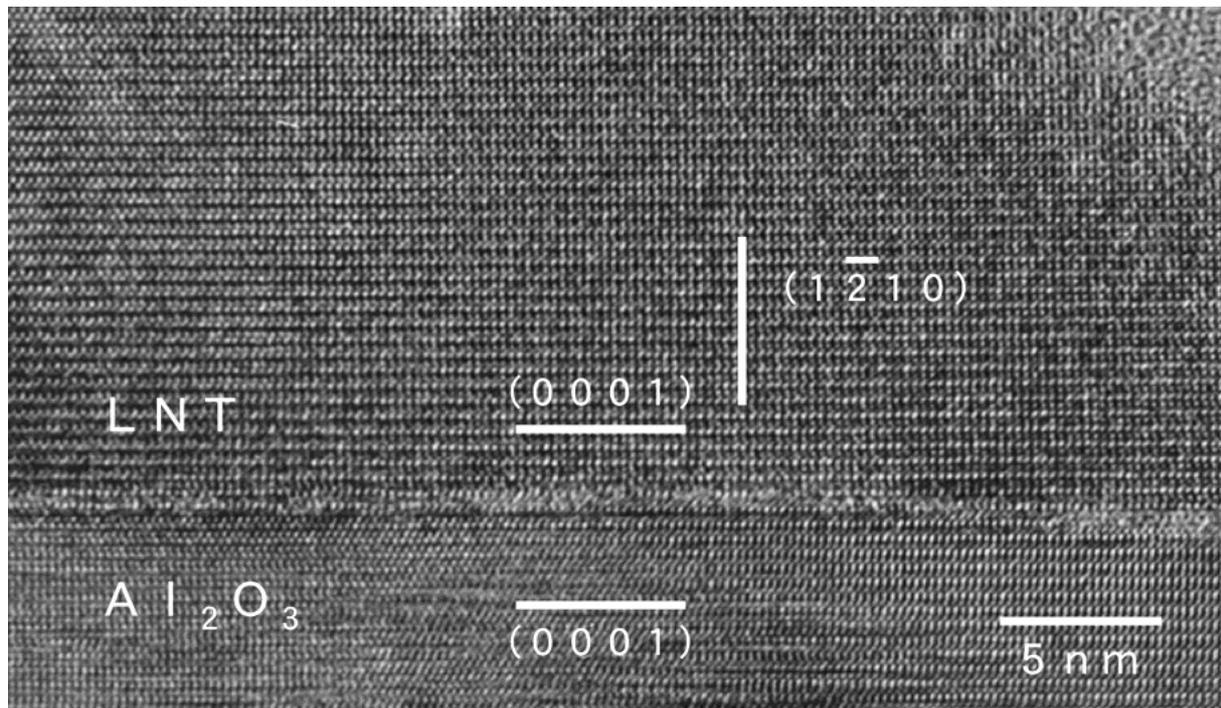In contrast, the film deposited at the feeding rate of

Fig. 3 HRTEM image of sample C, observed from the direction of $[10\bar{1}0]_{LNT}//[10\bar{1}0]_{Al_2O_3}$. In this figure, neither amorphous layer nor impurity phase are seen at the interface between the film and the substrate as well as in Fig. 2.
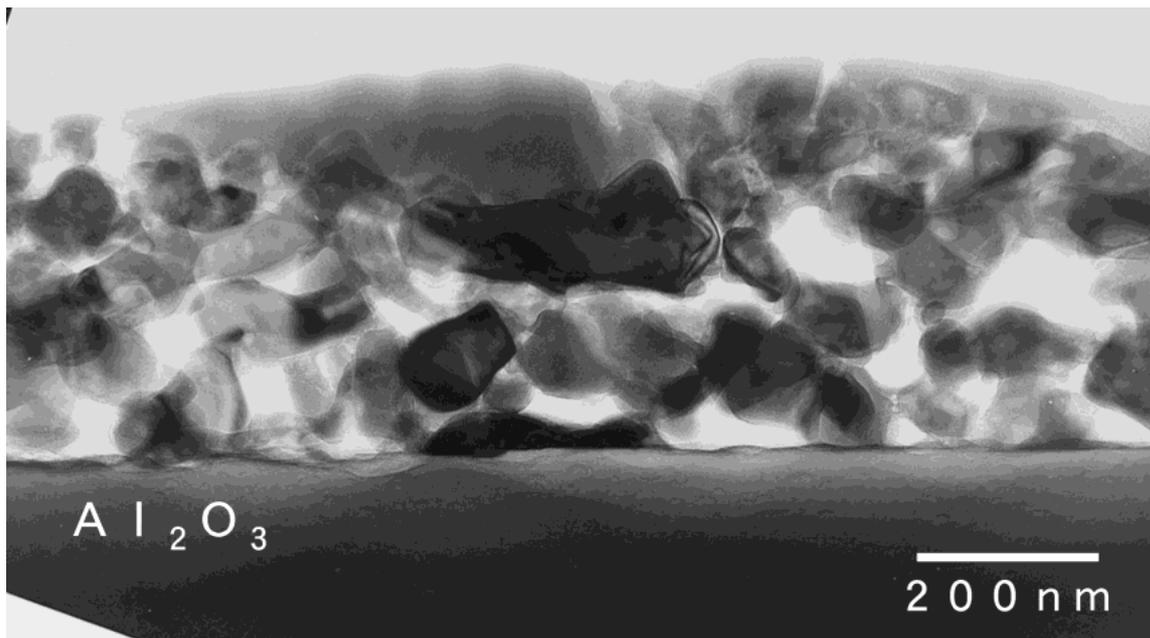


Fig. 4 Cross-sectional electron micrograph of sample A, taken along the direction of $[11\bar{2}0]_{Al_2O_3}$. It is noted that this film is polycrystalline.

0.5 mL/min was polycrystalline film containing mainly LNT crystals. As seen in the micrograph, amorphous phases and small pores are formed in the vicinity of the interface. Figure 4 shows a cross-sectional photograph of sample A, observed from $[11\bar{2}0]_{Al_2O_3}$.

Figures 5 show the cross-sectional view of sample B, observed from $[11\bar{2}0]_{Al_2O_3}$. This film included many twin crystals of LNT and other oriented LNT crystals. One of these twin crystals has the orientation relationship described in the formula (I), the other has the following orientation

relationship:

$$(0001)_{LNT}//(0001)_{Al_2O_3}, \quad [\bar{2}110]_{LNT}//[11\bar{2}0]_{Al_2O_3} \quad (II)$$

This orientation relationship (II) can be obtained by a rotation of $60°$ for the OR(I) about their common axis $[0001]_{LNT}//[0001]_{Al_2O_3}$.

In the case of sample D fabricated at the feeding rate of 10 mL/min, the twin crystals are frequently observed as shown in Fig. 6(a). Figures 6(a) and (b) show the cross-sectional micrographs of sample D, taken along the direction
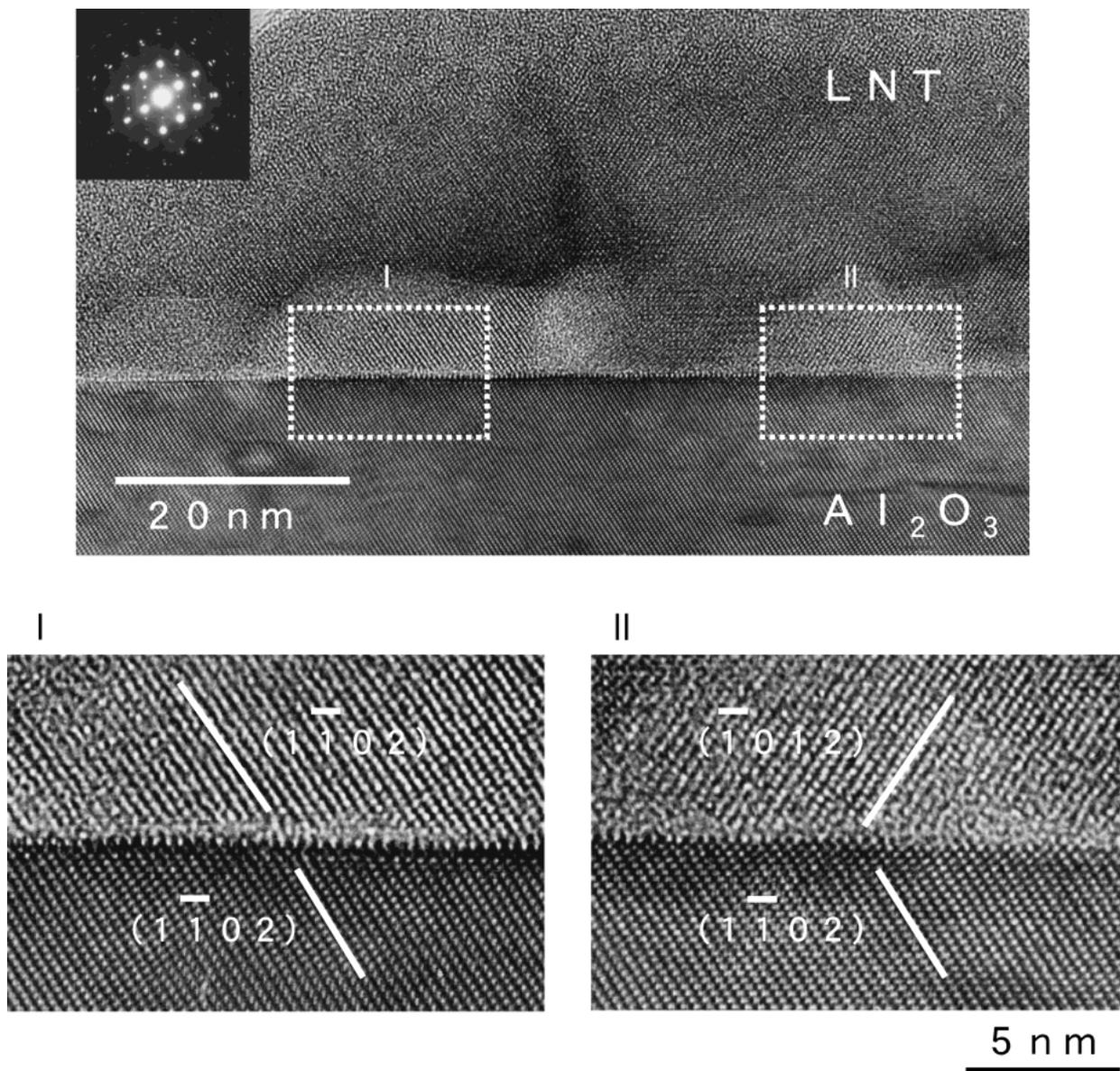
Fig. 5 Cross-sectional micrograph of sample B, observed from the direction of $[11\bar{2}0]_{Al_2O_3}$. In-plane orientation relationship of Part I is $[11\bar{2}0]_{LNT}//[11\bar{2}0]_{Al_2O_3}$. In contrast, that of Part II is $[\bar{2}110]_{LNT}//[11\bar{2}0]_{Al_2O_3}$, which is obtained by a rotation of 60° with respect to the direction of $[0001]_{LNT}//[0001]_{Al_2O_3}$. These relationships are symmetrical with respect to $(1\bar{1}00)_{LNT}$ plane.

of (a) $[11\bar{2}0]_{Al_2O_3}$ and (b) $[10\bar{1}0]_{Al_2O_3}$, respectively. Other phases such as Li(Nb, Ta)$_3$O$_8$ and other oriented LNT crystals such as $(10\bar{1}4)_{LNT}//(0001)_{Al_2O_3}$ are also seen.

Figures 7(a) and (b) show plan-view transmission electron micrographs of sample C and sample B respectively, taken from the direction of $[0001]_{Al_2O_3}$. As shown in these figures, the size of LNT grains in the sample C is larger than that in the sample B. Figure 7(c) shows the HRTEM image taken at a part of Fig. 7(a). Moiré fringes are seen due to the difference between distances of $(1\bar{2}10)_{LNT}$ and $(1\bar{2}10)_{Al_2O_3}$ planes. In addition, edge dislocations are observed as indicated by arrows, which are considered to be generated by coarsening of LNT grains during film deposition. It was reported that the size of the crystal nuclei generated on the surface of the substrate is larger, as the feeding rate is higher in the case of YBa$_2$Cu$_3$O$_{7-y}$ films deposited by the thermal plasma flash evaporation method.[16] In the present TEM observation, the

grain size in the LNT film was largest in the sample C deposited with the middle range of the feeding rate, as shown in the Figs. 7. Therefore, large grains in the LNT film of sample C were formed by diffusion and coarsening of the crystal nuclei. From a series of results, it seems that the relative rate of 'in-plane' growth to 'out-of-plane' growth determines the crystallinity of the film. In the case of slow feeding rate, the number of crystal nuclei, which is generated on the substrate, is not so much. Thus, the in-plane growth rate is slow and the crystallinity of the film is not expected to be good, if the diffusion rate of the LNT crystal nuclei is not so high. On the other hand, in the case of high feeding rate ($> 7$–$8$ mL/min), the growth rate of the film along the direction perpendicular to the surface of the substrate is much higher than the in-plane growth rate. As a result, orientation relationships between the films and the substrates tend to be random. The LNT film deposited at the feeding rate of 7 mL/min in the middle of the

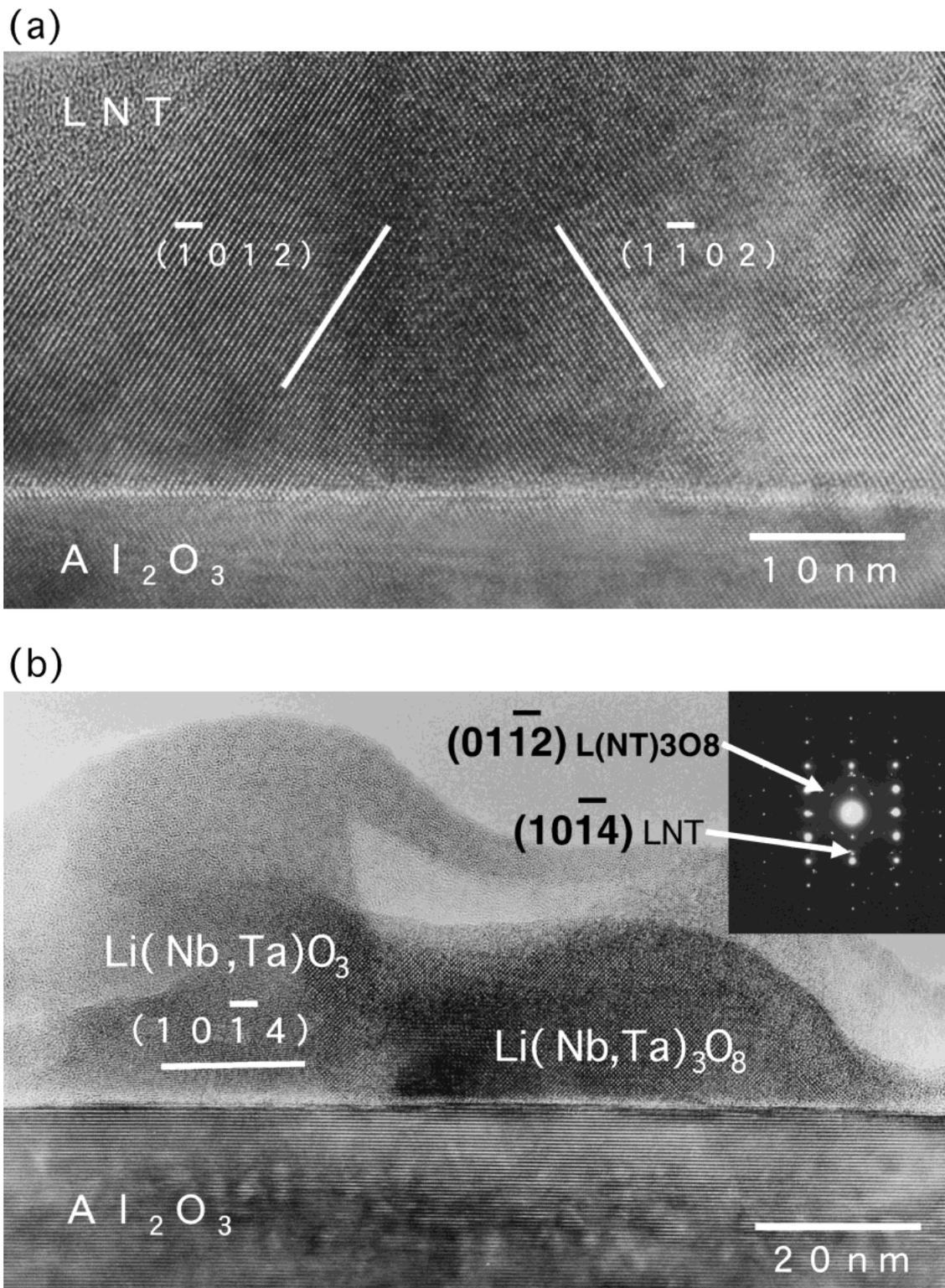Fig. 6 Cross-sectional micrographs of sample D, observed from the direction of (a) $[11\bar{2}0]_{Al_2O_3}$ and (b) $[10\bar{1}0]_{Al_2O_3}$. In this film, many twin crystals are observed, as shown in Fig. 6(a). In addition, other phases such as $Li(Nb,Ta)_3O_8$ and the LNT crystals with other orientation relationships such as $(10\bar{1}4)_{LNT}//(0001)_{Al_2O_3}$ are also seen.

range has good crystallinity and a unique orientation relationship.

### 3.2 Orientation relationship

A series of TEM observations revealed that the preferential orientation relationship between the LNT film and the $Al_2O_3$ substrate is described as the formula (I). The orientation relationship (II) was frequently observed in the sample B and sample D. These OR(I) and OR(II) are symmetrical with respect to $(1\bar{1}00)_{LNT}$ plane. The orientation relationship of $(10\bar{1}4)_{LNT}$ parallel to $(0001)_{Al_2O_3}$ was also seen in the sample D. All of these relationships are considered to depend on the
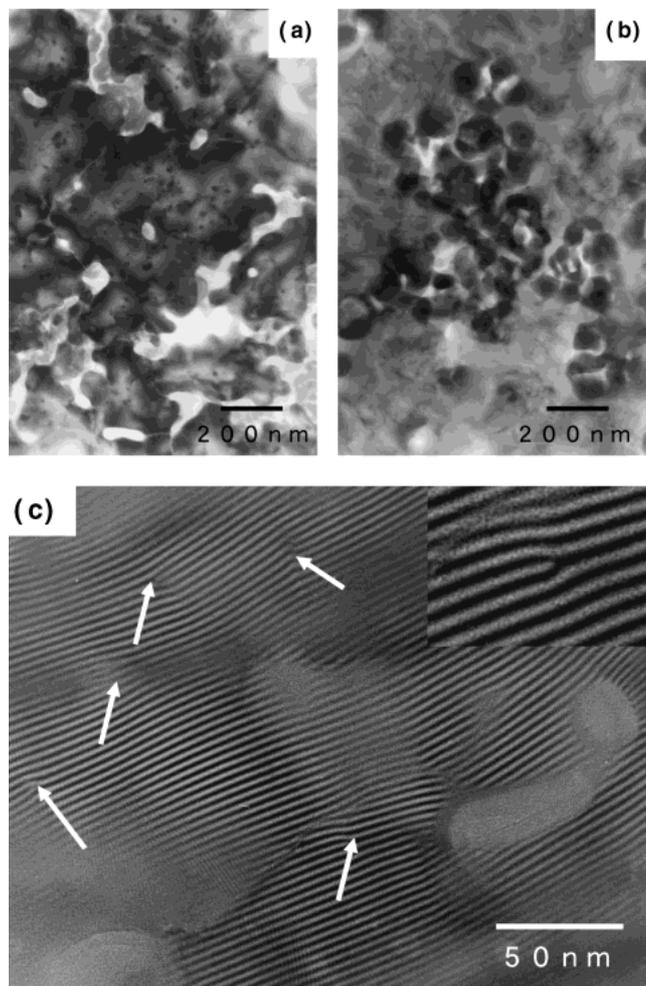
Fig. 7 Low-magnification plan-view micrographs of (a) sample C and (b) sample B, respectively. Figure 7(c) shows HRTEM image of sample C, taken at the same part of Fig. 7(a). Figures 7(a) and (b) were obtained just from the direction of $[0001]_{Al_2O_3}$. However, fig. 7(c) was taken along the direction inclined from $[0001]_{Al_2O_3}$.
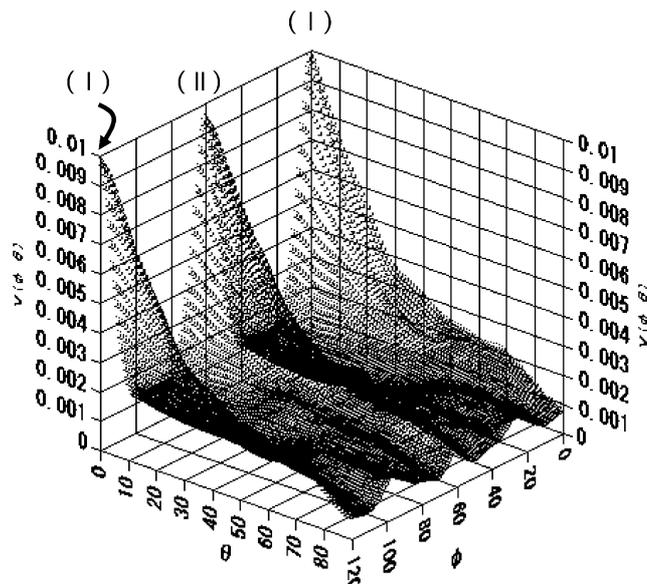


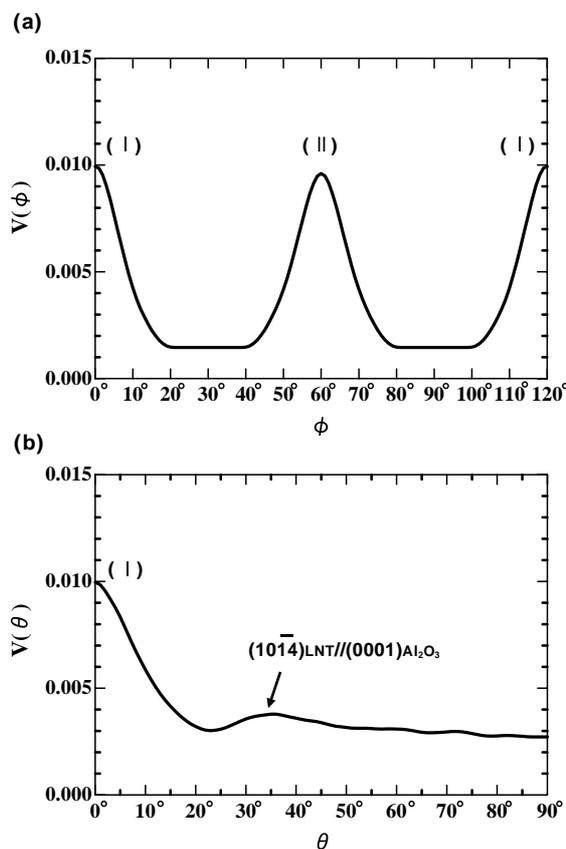Fig. 8 Three-dimensional plots of $V(\phi, \theta)$ versus $\phi$ and $\theta$ calculated by CRLP method for the LNT/Al$_2$O$_3$ system.



Fig. 9 Two-dimensional plots of $V(\phi)$ and $V(\theta)$ calculated by CRLP method for the LNT/Al$_2$O$_3$ system: (a) $V(\phi)$ plots corresponding to the section at $\theta = 0°$; (b) $V(\theta)$ plots corresponding to the section at $\phi = 0°$.

states of coherency between two lattices across the interface. Coincidence of reciprocal lattice points (CRLP) has been developed to elucidate a geometrical coherency and to predict an optimum relationship between the film and the substrate.[22,23] In this method, the geometrical model is applied to clarify the orientation relationship, the overlap of reciprocal lattice points (RLP) of two adjoining crystals is calculated to obtain the optimum OR between two crystals. The basis of the model is that the optimum OR corresponds to a situation where the two lattices best accommodate each other and thus result in the lowest strain energy- and a minimum total energy for the system as a whole.

Figure 8 shows a three dimensional plots $V(\phi, \theta)$ versus $\phi$ and $\theta$ for this LNT/Al$_2$O$_3$ system; exhibiting some predominant peaks. The initial orientation relationship ($\phi, \theta = 0°$) was set to $(0001)_{LNT}//(0001)_{Al_2O_3}$ and $[11\bar{2}0]_{LNT}//[11\bar{2}0]_{Al_2O_3}$. $\Phi$ and $\theta$ are rotation angles around $[0001]$ and $[10\bar{1}0]$ of Al$_2$O$_3$, respectively. Figure 9(a) is the two-dimensional $V(\phi)$ plots corresponding to section of Fig. 8 at $\theta = 0°$. It is clearly seen that the peak is periodic in $\phi$ with the periodicity of 60°. However, the peak at 60° which corresponds to the OR(II), is slightly lower than

those at 0° and 120° for the OR(I). Figure 9(b) shows the two-dimensional $V(\theta)$ plots corresponding to the section of Fig. 8 at $\phi = 0°$. Small peak at $\theta = 35°$ in this figure coincides to the OR of $(10\bar{1}4)_{LNT}//(0001)_{Al_2O_3}$, which was observed in the sample D.

From this result, we confirmed that the orientation relationships observed by TEM correspond to the states where the

two lattices accommodate each other and result in the lowest strain energy. In such a system with large lattice mismatch, a set of the geometrical misfit dislocations harmonizes the mismatch between the lattices of the film and the substrate from the very initial stages of growth.

## 4.  Conclusions

LNT films were deposited by thermal plasma spray CVD method at various feeding rates of liquid raw materials, and their cross sections and plan views were investigated by means of transmission electron microscopy (TEM). It was found that the optimum feeding rate for achieving epitaxial growth and good crystallinity of the LNT films was 7 mL/min in the middle of the range from 0.5 to 10 mL/min. At that time, the orientation relationship between the film and the substrate was $(0001)_{LNT}//(0001)_{sapphire}$, $[11\bar{2}0]_{LNT}//[11\bar{2}0]_{sapphire}$. In the cases of the higher and lower feeding rate, LNT films included twin crystals and other phases such as $Li(Nb, Ta)_3O_8$. The calculation based on the coincidence of reciprocal lattice points revealed that the orientation relationship observed experimentally by TEM corresponds to the states where the two lattices accommodate each other and result in the lowest strain energy.

## Acknowledgments

## REFERENCES

1) A. Yamada, H. Tamada and M. Saitoh: Appl. Phys. Lett. **61** (1992) 2848–2850.
2) S. Y. Lee and R. S. Feigelson: J. Mater. Res. **14**(6) (1999) 2662–2667.
3) K. Shiratsuyu, A. Sakurai, K. Tanaka and Y. Sakabe: Jpn. J. Appl. Phys. **38** (1999) 5437–5441.
4) S. B. Ogale, R. N. Dikshit, S. J. Dikshit and S. M. Kanetkar: J. Appl. Phys. **71** (1992) 5718–5720.
5) A. M. Marsh, S. D. Harkness, F. Qian and R. K. Singh: Appl. Phys. Lett. **62** (1993) 952–954.
6) S.-H. Lee, T. K. Song, T. W. Noh and J.-H. Lee: Appl. Phys. Lett. **67** (1995) 43–45.
7) F. Veignant, M. Gandais, P. Aubert and G. Garry: Thin Solid Films **336** (1998) 163–167.
8) F. Veignant, M. Gandais, P. Aubert and G. Garry: J. Cryst. Growth **196** (1999) 141–150.
9) K. Nashimoto, M. J. Cima, P. C. McIntyre and W. E. Rhine: J. Mater. Res. **10** (1995) 2564–2572.
10) K. Terabe, N. Iyi, K. Kitamura and S. Kimura: J. Mater. Res. **10** (1995) 1779–1783.
11) K. Terabe, A. Gruverman, Y. Matsui, N. Iyi and K. Kitamura: J. Mater. Res. **11** (1996) 3152–3157.
12) T. A. Rost, H. Lin, T. A. Rabson, R. C. Baumann and D. L. Callahan: J. Appl. Phys. **72** (1992) 4336–4343.
13) T. Kawaguchi, H. Kitayama, M. Imaeda, S. Ito, K. Kaigawa, T. Taniuchi and T. Fukuda: J. Cryst. Growth **169** (1996) 94–97.
14) S. D. Cheng, C. H. Kam, Y. Zhou, X. Q. Han, W. X. Que, Y. L. Lam, Y. C. Chan, J. T. Oh and W. S. Gan: Thin Solid Films **365** (2000) 77–81.
15) K. Terashima, K. Eguchi, T. Yoshida and K. Arashi: Appl. Phys. Lett. **52** (1988) 1274–1276.
16) Y. Takamura, Y. Hirokawa, H. Komaki, K. Terashima and T. Yoshida: Physica C **190** (1991) 122–123.
17) K. Terashima, T. Akagi, H. Komaki and T. Yoshida: J. Appl. Phys. **71** (1992) 3427–3430.
18) N. Yamaguchi, T. Hattori, K. Terashima and T. Yoshida: Thin Solid Films **316** (1998) 185–188.
19) T. Majima, H. Yamamoto, S. A. Kulinich and K. Terashima: J. Cryst. Growth **220** (2000) 336–340.
20) H. Yamamoto, S. A. Kulinich and K. Terashima: Thin Solid Films **390** (2001) 1–6.
21) Y. Ikuhara, P. Pirouz, A. H. Heuer, S. Yadavalli and C. P. Flynn: Philos. Mag. A **70** (1994) 75–97.
22) Y. Ikuhara and P. Pirouz: Microscopy Research and Technique **40** (1998) 206–241.
23) Y. Ikuhara and P. Pirouz: Mater. Sci. Forum **207–209** (1996) 121–124.